REPORT SRL 01-F-1989

SCALING DISCHARGE PUMPED RARE GAS LASERS AND ULTRA-HIGH AVERAGE POWER

Prepared by
Dr. Jonah Jacob
Dr. Reich Watterson

SCIENCE RESEARCH LABORATORY, INC.
15 Ward Street
Somerville, MA 02143

17 January 1989

FINAL TECHNICAL REPORT
Period for July 13, 1988 to January 12, 1989
Contract Number DASG60-88-C-0052

APPROVED FOR PUBLIC RELEASE; DISTRIBUTION UNLIMITED

Sponsored by
SDIO/Innovative Science and Technology Office

Managed by
U. S. Army Strategic Defense Command

Unclassified
SECURITY CLASSIFICATION OF THIS PAGE

REPORT DOCUMENTATION PAGE

Form Approved
OMB No. 0704-0188
Exp. Date: Jun 30, 1986

1a. REPORT SECURITY CLASSIFICATION
Unclassified

1b. RESTRICTIVE MARKINGS

2a. SECURITY CLASSIFICATION AUTHORITY

2b. DECLASSIFICATION / DOWNGRADING SCHEDULE

3. DISTRIBUTION / AVAILABILITY OF REPORT
Approved for Public Release; Distribution Unlimited

4. PERFORMING ORGANIZATION REPORT NUMBER(S)
SRL 01-F-1989

5. MONITORING ORGANIZATION REPORT NUMBER(S)
W31RPD

6a. NAME OF PERFORMING ORGANIZATION
Science Research Laboratory

6b. OFFICE SYMBOL (If applicable)

7a. NAME OF MONITORING ORGANIZATION
U.S. Army Strategic Defense Command

6c. ADDRESS (City, State, and ZIP Code)
15 Ward St., Somerville, MA 02143

7b. ADDRESS (City, State, and ZIP Code)
P.O. Box 1500
Huntsville, AL 35807-3801

8a. NAME OF FUNDING / SPONSORING ORGANIZATION
SDIO/Innovative Science & Technology Office

8b. OFFICE SYMBOL (If applicable)

9. PROCUREMENT INSTRUMENT IDENTIFICATION NUMBER
DASG60-88-C-0052

8c. ADDRESS (City, State, and ZIP Code)
Pentagon
Washington, DC

10. SOURCE OF FUNDING NUMBERS

PROGRAM ELEMENT NO.	PROJECT NO.	TASK NO.	WORK UNIT ACCESSION NO.
	CARN: 8C1303		

11. TITLE (Include Security Classification)
Scaling Discharge Pumped Rare Gas Lasers to Ultra-High Average Power

12. PERSONAL AUTHOR(S)
Jacob, Jonah and Watterson, Reich

13a. TYPE OF REPORT	13b. TIME COVERED	14. DATE OF REPORT (Year, Month, Day)	15. PAGE COUNT
Final	FROM 7/13/88 TO 1/12/89	89/1/12	37

16. SUPPLEMENTARY NOTATION

17. COSATI CODES		
FIELD	GROUP	SUB-GROUP

18. SUBJECT TERMS (Continue on reverse if necessary and identify by block number)
Rare Gas, Short Wavelength Laser, High Pressure Discharge

19. ABSTRACT (Continue on reverse if necessary and identify by block number)

Discharge pumped rare gases have been made to lase on a number of transitions from 0.63 μm in the visible to 4 μm in the IR. Most of these lasers have operated in low pressure discharges with efficiences of < 1%. Soviet scientists at the Lebedev Institute obtained an intrinsic efficiency of 5% at 1.73μm in an electron beam controlled discharge. The laser mixture was Ar/Xe at total pressures of 1-4 atmospheres. More recently several groups in the US including SRL, have obtained efficient lasing action in atmospheric pressure Ar/Xe mixtures. These lasers offer several advantages including: high duty factor waveforms which will eliminate the effects of stimulated Raman Scattering on atmospheric propagation, no fuel burnup, and high specific energy extraction (50 J/L) resulting in compact, inexpensive laser devices. The key issue to be addressed before the potential of these lasers can be realized is the stability of the laser discharge for long pulse durations at the required power densities. This issue has been investigated theoretically during Phase I of this effort. SRL has also developed a laser kinetic model for the Ar/Xe laser. Both the discharge and laser kinetic models will be presented in this report.

20. DISTRIBUTION / AVAILABILITY OF ABSTRACT
☒ UNCLASSIFIED/UNLIMITED ☐ SAME AS RPT. ☐ DTIC USERS

21. ABSTRACT SECURITY CLASSIFICATION
Unclassified

22a. NAME OF RESPONSIBLE INDIVIDUAL

22b. TELEPHONE (Include Area Code)

22c. OFFICE SYMBOL

DD FORM 1473, 84 MAR

83 APR edition may be used until exhausted.
All other editions are obsolete.

SECURITY CLASSIFICATION OF THIS PAGE
Unclassified

TABLE OF CONTENTS

LIST OF ILLUSTRATIONS

1.0 INTRODUCTION

SDIO has considerable interest in developing efficient short wavelength Ground Based Lasers (GBLs) for defense against ballistic missiles. To date, SDIO has pursued primarily two GBL laser technologies - excimers and FELs. In this proposal, Science Research Laboratory (SRL) identifies an alternate GBL concept based on electron beam controlled discharge pumped rare gas lasers. These lasers have overall system efficiencies that are potentially a factor of 2 greater than excimer lasers and can potentially be scaled to the multi- megawatt average power levels required for strategic defense applications. Other advantages of these laser systems are listed below.

- These lasers have known transitions in atmospheric windows. Therefore Raman-shifting the laser wavelength to wavelengths that can propagate more easily through the atmosphere - a process which results in decreased laser system efficiency - is not required. For example the EMRLD XeF laser at 351 nm is 2 - 3% efficient. However incorporating a Raman shift to the required 411 nm wavelength results in a decrease in efficiency by about 50%.
- With electron beam controlled discharge pumping of rare gas lasers, most of the power and energy for exciting the laser transition comes from the discharge. This can be compared to excimer lasers in which all of the power and energy for the laser comes from an electron beam. The electron beam has to be generated in a vacuum and transmitted through a thin metallic foil to the high pressure laser medium. As a result, a significant efficiency loss is experienced in transporting the electron beam through the foil and its support structure. The fact that most of the power for pumping rare gas lasers comes from the discharge which is controlled by a relatively low current density electron beam alleviates the electron beam transmission loss as well as foil cooling and foil life issues.
- No fuel burnup - Unlike excimer lasers, these lasers do not depend on halogens or other fuels that are depleted by laser operation. Hence these laser systems are

capable of long pulse operation and high duty factors without gas processing and replenishment. Long pulse lengths result in a significantly lower peak power (at a given average power) which eliminates atmospheric Raman scattering losses on both the uplink and downlink. Further the gases are inert and nontoxic and so chemical scrubbing and special handling are not necessary.

- Laser action occurs between allowed atomic transitions and so the gain is high and optical absorption of the laser medium at the laser wavelength is less important. Therefore these lasers can be potentially scaled to ultra-high average power ($>$ 100 MW) from a single aperture. This feature will significantly reduce the cost of the laser system.
- Efficient laser transitions in rare gas mixtures occur between 0.6 - 4 μm. At these wavelengths the turbulence in the atmosphere has a larger correlation length than in the ultraviolet thereby reducing the number of channels required in the adaptive optics system. Further at these longer wavelengths, optical damage thresholds are higher and atmospheric transmission efficiency is higher. These factors, taken together, more than compensate for the increased diffractive spreading of the uplink laser beam in terms of overall system cost.
- These lasers also have the capability of delivering large specific energies ($\geq$ 50 J/liter) which will result in relatively compact and inexpensive ground based laser devices.

The key issues which must be addressed before the potential of these lasers can be realized is the stability of the discharge as a function of discharge pump power density and pulse length. The best results to date have been obtained by Soviet scientists at the Lebedev Institute.[1] They extracted 80 Joules in a 30 μs pulse from a 5 liter active volume. More recently several groups in the US have obtained efficient lasing action in Ar/Xe mixtures.[2,3,4] The most efficient and longest pulse data has been obtained by the scientists at Sandia National Laboratory.[2] By nuclear reactor pumping they have

measured power efficiencies of 6% and millisecond laser pulse lengths. The Soviet electron beam controlled discharge laser result is significant in so far as the specific energy is twice as large as excimer lasers and the pulse length is more than a factor of ten longer than that achievable with XeF and XeCl lasers. Therefore, the same average power can be obtained from a laser which has less than half the active volume of an excimer laser. The increased pulse length will lower the peak intensity by two orders of magnitude thereby eliminating problems associated with stimulated Raman scattering in the atmosphere. Science Research Laboratory (SRL) believes that the Soviet results can be extended to longer pulse lengths (100μsec) resulting in larger energy extracted per unit volume (50 J/liter) and shorter wavelengths in the range between 0.6 to 2.0 μm to minimize diffractive losses. The key to realizing these performance improvements in lasers based on rare gas mixtures is to develop stable electron beam controlled discharge pumping at high pressure. This key technical issues was addressed theoretically in Phase I by developing a detailed kinetic and discharge models for these lasers.

The relevant energy levels for xenon rare gas lasers are shown in Fig. 1. Also shown in Fig. 1 are the most efficient laser transitions observed to date. Table 1 gives a more detailed list of transitions that have lased together with the transmission efficiency through a 3 km standard atmosphere for laser radiation at each transition. Transmission losses for this path are approximately equivalent to the uplink loss for a GBL located at sea level. The transmission efficiency predictions of Table 1 are based on high resolution atmospheric propagation modeling obtained with FASCODE. All transitions listed have acceptably high transmission except for the $5d(5/2)^0_3 \rightarrow 6p(5/2)_3$ transition at 2.48 μm. There exist many other shorter wavelength laser transitions in neon and krypton rare gas mixtures which may be efficiently accessed at high pressure with electron beam controlled discharge pumping.

2.0 ELECTRON BEAM CONTROLLED DISCHARGE EXCITATION OF RARE GAS LASERS

There are many combinations of rare gases such as He/Ne, Kr/Xe and Ar/Xe which

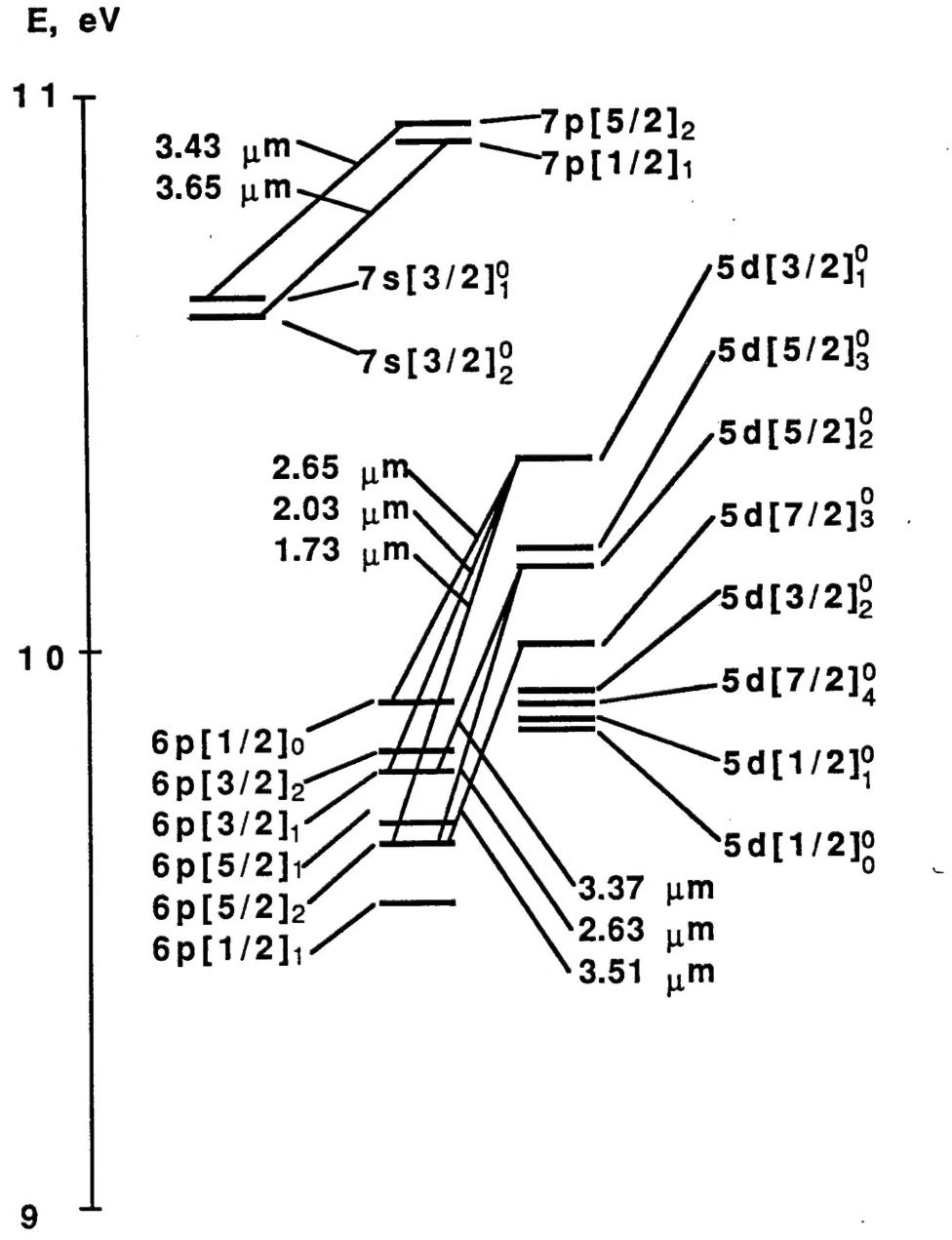

Figure 1: Observed laser transitions in Xe-rare gas mixtures.

TABLE I

TRANSMISSION OF VARIOUS Xe LASER LINES THROUGH 3 km OF ATMOSPHERE AT 200 ft ALTITUDE (FASCODE)

WAVELENGTH μM	TRANSITION ASSIGNMENT	STANDARD ATMOSPHERE %
1.733	$5d[3/2]^0_1 \rightarrow 6p[5/2]_2$	72
2.026	$5d[3/2]^0_1 \rightarrow 6p[5/2]_1$	65
2.482	$5d[5/2]^0_3 \rightarrow 6p[5/2]_3$	43
3.367	$5d[5/2]^0_2 \rightarrow 6p[3/2]_1$	63
3.434	$7p[5/2]_2 \rightarrow 7s[3/2]^0_1$	63
3.507	$5d[7/2]^0_3 \rightarrow 6p[5/2]_2$	72
3.6219	$5d[3/2]^0_2 \rightarrow 7p[3/2]_2$	83
3.6518	$7p[1/2]_1 \rightarrow 7s[3/2]^0_2$	84
3.679	$5d[1/2]^0_1 \rightarrow 6p[1/2]_1$	74
3.685	$5d[5/2]^0_2 \rightarrow 6p[3/2]_2$	81
3.869	$5d[5/2]^0_2 \rightarrow 6p'[3/2]_3$	82
3.895	$5d[7/2]^0_2 \rightarrow 6p[5/2]_3$	84
3.996	$5d[1/2]^0_0 \rightarrow 6p[1/2]_1$	85
4.021	$7p[1/2]_1 \rightarrow 7s[3/2]^0_1$	82
4.15	$5d'[5/2]^0_2 \rightarrow 7p[3/2]_1$	83

can lead to efficient, scalable short wavelength laser operation at atmospheric pressure. For the remainder of this section, electron beam controlled discharge pumping of the Ar/Xe laser will be discussed in some detail. The reason Ar/Xe is chosen as an example is that this combination of rare gases has recently achieved an intrinsic efficiency of 5% in laser experiments at 1.73 μm [1,2,3]and there exists experimental data on high pressure electron beam controlled discharges in the Soviet literature[1] which indicates that stable discharge operation can be sustained for $\geq$ 30 μsec pulse lengths at the required pump power density. More Recently various groups in the United States [2,3] including SRL have obtained efficient lasing action in Ar/Xe. From this data one can obtain a better understanding of this laser. In fact scientists at SRL have developed a model that successfully explains their results. These results and model will be presented later in this proposal.

The upper levels of Ar/Xe lasers are within the Xe* (5d) manifold (see Fig. 1) which lies from 10 to 11 eV above the ground state of xenon. The resulting IR laser photon energy is between 0.3 - 0.7 eV, so if these levels are created by direct electron impact the intrinsic efficiency would have been much less than the 5 percent measured by the various groups that are investigating these lasers. To explain their high intrinsic efficiencies, the Lebedev group have postulated creation of a low level population of Xe* metastable levels with a low current, high energy electron beam. The low voltage, high current discharge then ionizes these states by multiple electron impact and the upper laser level is populated by molecular ion-electron recombination. This process is shown schematically in Fig. 2. Typically the power deposited by the electron beam, which is eventually channeled to provide the required population of Xe*, is 1-2% of the power deposited by the discharge.

3.0 PHYSICS OF DISCHARGE PUMPING

In this section a brief discussion of the physics of electron beam controlled discharge pumping of Ar/Xe lasers will be presented. The high energy beam electrons e_h deposit most of their energy into the formation of electron- ion pairs via the following reaction

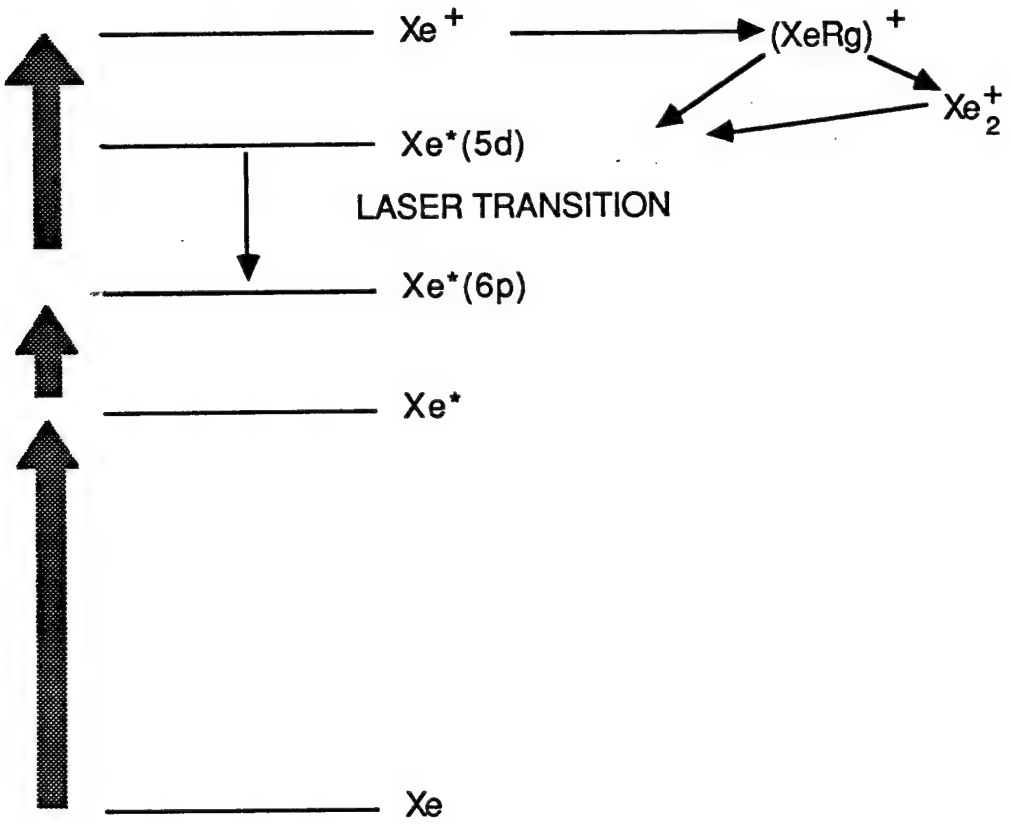

Figure 2: Schematic of the pertinent energy levels of Xenon High Efficiency in rare gas/Xenon lasers is achieved by recycling Xe* several times before decay to the ground.

$$e_h + Ar \rightarrow Ar^+ + e + e_h \tag{1}$$

The atomic argon ions Ar^+ rapidly form molecular ions Ar_2^+ by a three body collision process

$$Ar^+ + 2Ar \rightarrow Ar_2^+ + Ar \tag{2}$$

The molecular ions create xenon atomic ions by charge transfer collisions

$$Ar_2^+ + Xe \rightarrow Xe^+ + 2Ar \tag{3}$$

The Xe ions then form molecular ions Xe_2^+ which rapidly recombine with electrons to form xenon metastables Xe^*

$$Xe_2^+ + e \rightarrow Xe^*(5d) + Xe \tag{4}$$

which then lase on the $5d \rightarrow 6p$ transition at 1.73 μm.

$$h\nu + Xe^*(5d) \rightarrow Xe^*(6p) + 2h\nu$$

Once formed, the lower lying metastables of xenon will be efficiently ionized by multi-step electron impact in the following set of reactions

$$\begin{aligned} e + Xe^* &\rightarrow Xe^{**} + e \\ e + Xe^* &\rightarrow Xe^+ + 2e \end{aligned} \tag{5}$$

$$\begin{aligned} e + Xe^{**} &\rightarrow Xe^{***} + e \\ e + Xe^{**} &\rightarrow Xe^+ + 2e \end{aligned} \tag{6}$$

$$e + Xe^{***} \rightarrow Xe^+ + 2e \tag{7}$$

Since the spacing between the manifold of excited states above the metastable state is less than 1.6 eV, the reactions (5), (6) and (7) are driven by the low energy core of the electron distribution. The fact that most of the electrons can excite Xe^* to higher lying levels, coupled with the large electron impact cross sections for pumping the excited states up the energy level ladder, insures that reactions (5), (6) and (7) proceed efficiently and rapidly.

The upper laser level is formed through the ionic channel as shown in Fig. 2. Once Xe^+ is formed via the multistep process, it can recombine rapidly by three body processes to form heteronuclear ions and xenon molecular ions via the following reactions.

$$Xe^+ + 2\,Ar \rightarrow XeAr^+ + Ar \tag{8}$$

$$XeAr^+ + Xe \rightarrow Xe_2^+ + Ar \tag{9}$$

The molecular ions then recombine with electrons to form Xe^* as shown in reaction (4).

The laser discharge characteristics for a multi-megawatt Ar:Xe laser are given in Table 2. The results from the Lebedev Institute suggest that the optimum gas mixture is 99% Ar and 1% Xe at a total pressure of 3 atm. The input power per unit volume required for efficient lasing has been estimated from the results of the Lebedev research to be 10^4 W/cm^3. So for a discharge electric field of 600 V/cm, a discharge current density of 16 A/cm^2 is required and the corresponding electron density is 3×10^{14} cm^{-3}. The laser discharge pulse length is assumed to be 100 μs which is three times longer than that obtained by the Soviet scientists.

A Boltzmann electron transport code, which calculates the steady state electron energy distribution function, was used to determine quantitatively the efficiency and electron impact excitation rate constant for pumping Xe^* up the energy level ladder. The predicted efficiency and excitation rate constant are plotted in Fig. 3, 4 and 5 as a function of the Xe^* density for a 99:1 mixture of Ar/Xe at a total pressure of one atmosphere. From

TABLE 2

• DISCHARGE CHARACTERISTICS	
GAS MIXTURE	Ar/Xe 99/1
TOTAL PRESSURE	3 atm
ELECTRIC FIELD	600 V/cm
CURRENT DENSITY	16 A/cm^2
DISCHARGE PULSE LENGTH	100 μsec
SPECIFIC ENERGY	10^3 J/L
DISCHARGE CURRENT	5.7 MA
DISCHARGE VOLTAGE	120 kV
DISCHARGE IMPEDANCE	2×10^{-2} Ω
• E-BEAM CHARACTERISTICS	
E-BEAM VOLTAGE	2 MV
CURRENT DENSITY	0.20 A/cm^2
PULSE LENGTH	100 μs
PULSE REPETITION RATE	30 Hz
DUTY FACTOR	10^{-2}
POWER DEPOSITED IN FOIL	12 W/cm^2
E-BEAM IMPEDANCE	200 Ω
GUIDE MAGNETIC FIELD	8 KG
• LASER CHARACTERISTICS	
WAVELENGTH	1.73 μm
SINGLE PULSE ENERGY	3.6×10^6 Joules
SPECIFIC ENERGY	50 J/liter
PULSE LENGTH	100 μs
AVERAGE POWER	100 MW
NONSATURABLE ABSORPTION	7×10^{-5} cm^{-1}
SATURATION FLUX	44 kW/cm^2
SMALL SIGNAL GAIN	0.06 cm^{-1}
INTRINSIC EFFICIENCY	5%
ACTIVE VOLUME	1.2 x 2 x 30 m^3
OPTICAL COATINGS	
- SINGLE PULSE FLUENCE INCIDENT	150 J/cm^2
- AVERAGE INTENSITY INCIDENT	4 kW/cm^2

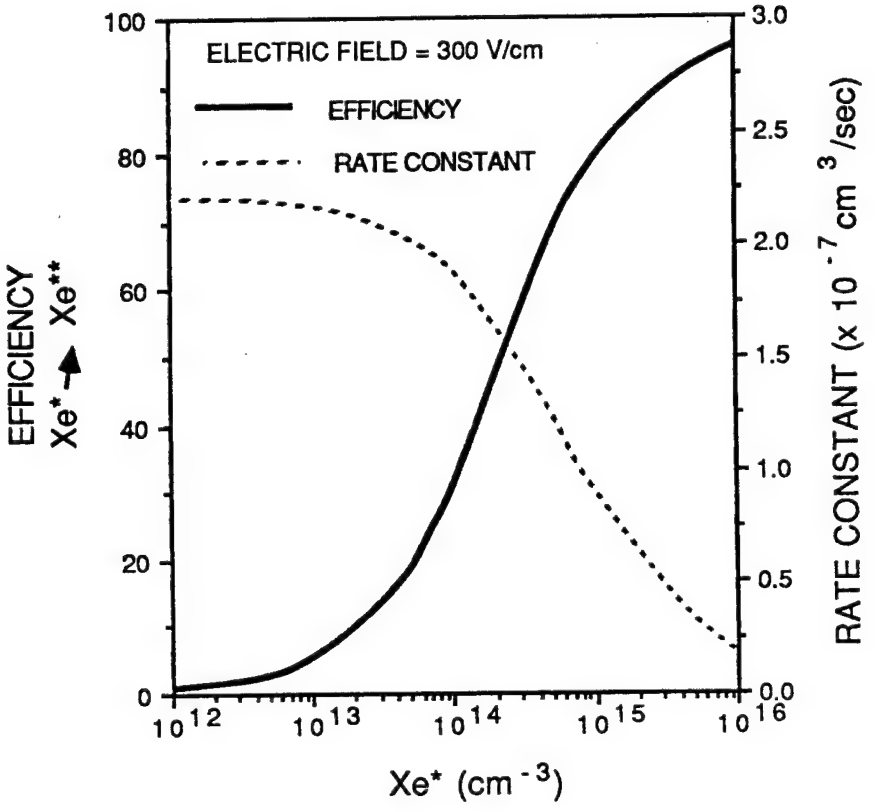

Figure 3: Curves showing the efficiency and rate constant for electron impact excitation of Xe* → Xe** in a 3 atmosphere Ar/Xe mixture containing 99% Ar and 1% Xe. The applied electric field is 300 V/cm.

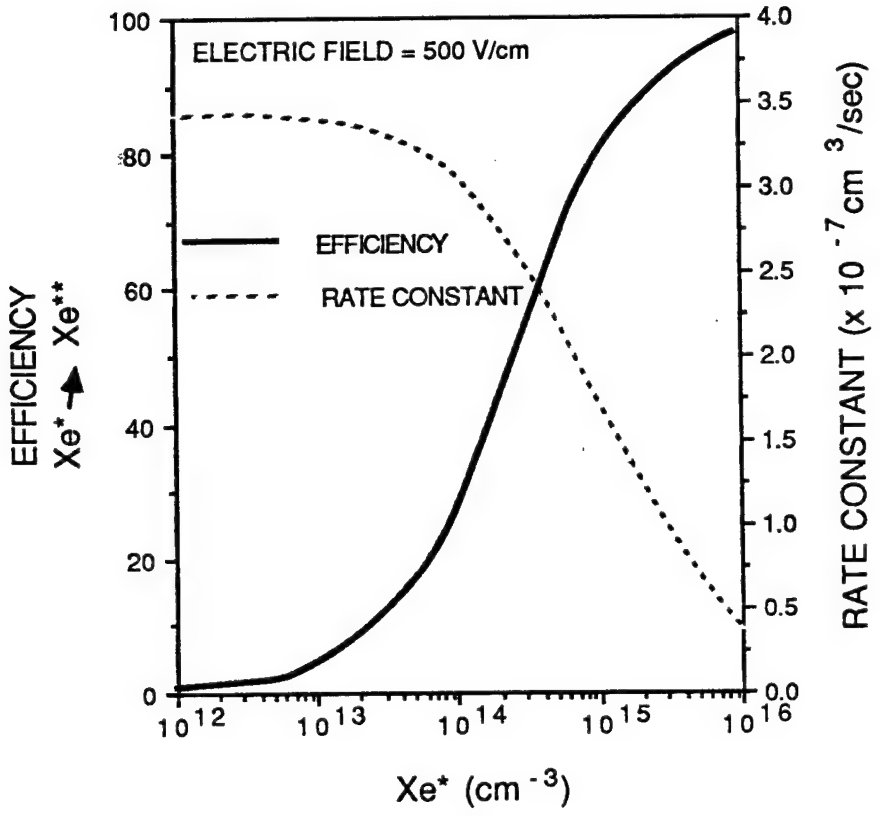

Figure 4: Curves showing the efficiency and rate constant for electron impact excitation of Xe* → Xe** in a 3 atmosphere Ar/Xe mixture containing 99% Ar and 1% Xe. The applied electric field is 500 V/cm.

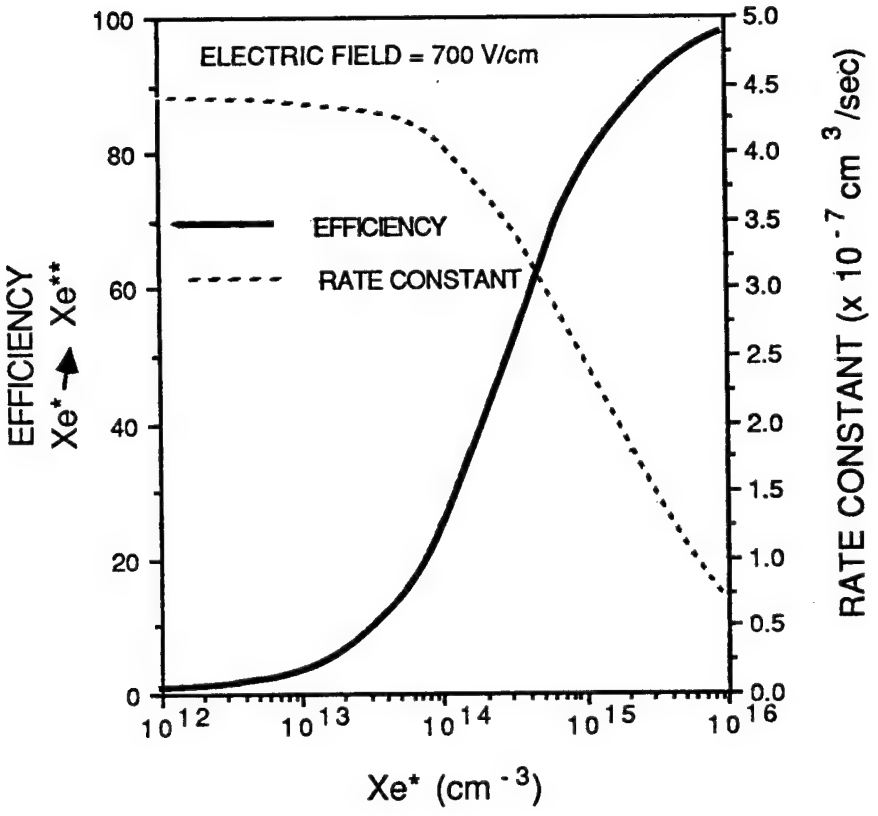

Figure 5: Curves showing the efficiency and rate constant for electron impact excitation of Xe* → Xe** in a 3 atmosphere Ar/Xe mixture containing 99% Ar and 1% Xe. The applied electric field is 700 V/cm.

Fig. 6 which shows the drift velocity V_d as a function of electric field it is clear that the current density increases very slightly over this range of electric field. The current density is proportional to the product of ($n_e v_d$). For the proposed electric field of 600 V/cm or 200 V/cm-atm. The efficiency of exciting Xe^* up the ladder can be high (>30%) provided the metastable density is . 10^{14} cm^{-3}. For these reasons, SRL proposes operating at the larger specific electric field of 200 V/cm atm which gives an electric field of 600 V/cm at mixture pressures of 3 atmosphere.

The high energy electron beam current density should be large enough to insure that the initial Xe^* density is approximately 10^{14} cm^{-3} and the electron density is $\simeq 3 \times 10^{14}$ cm^{-3}.

4.0 CONSIDERATION IN SCALING TO HIGH AVERAGE POWER

From the laser characteristics listed in Table 2, one sees that it is possible to extract 50 Joules/liter from the Ar/Xe laser if discharge stability can be maintained for a 100 μsec pulse length. To provide 3.6×10^6 J/pulse output energy, requires 7.2×10^4 liters of active laser volume. Assuming a gain length of 30 m and an electron beam height of 1.2 m, a flow width of 2m would be required. For such an electron beam height and at a pulse repetition rate of 30 Hz, a laser medium flow velocity of 1.1×10^4 cm/sec (M0.3) will be adequate to insure that the acoustic and entropy waves generated by discharge energy deposited in the laser medium will be totally cleared by flowing gas before the next pulse. A flow width of 1.2m determines that the e-beam energy must be 2MeV to insure that the electron beam and the discharge deposit power uniformly in the active medium. Such a laser will be capable of delivering an average power of 100 MW from a single device which is 30 m in length with the possibility of scaling to even higher average power.

Optical gain within the narrowline rare gas laser transitions is large and it has been verified that the gain coefficient is substantially larger than the nonsaturable absorption coefficient, α_{NR}. In fact using the measured value of α_{NR} for these conditions given in Table 2 one can estimate that α_{NR} L $\simeq$0.2 for a 30 m gain length and efficient length scaling

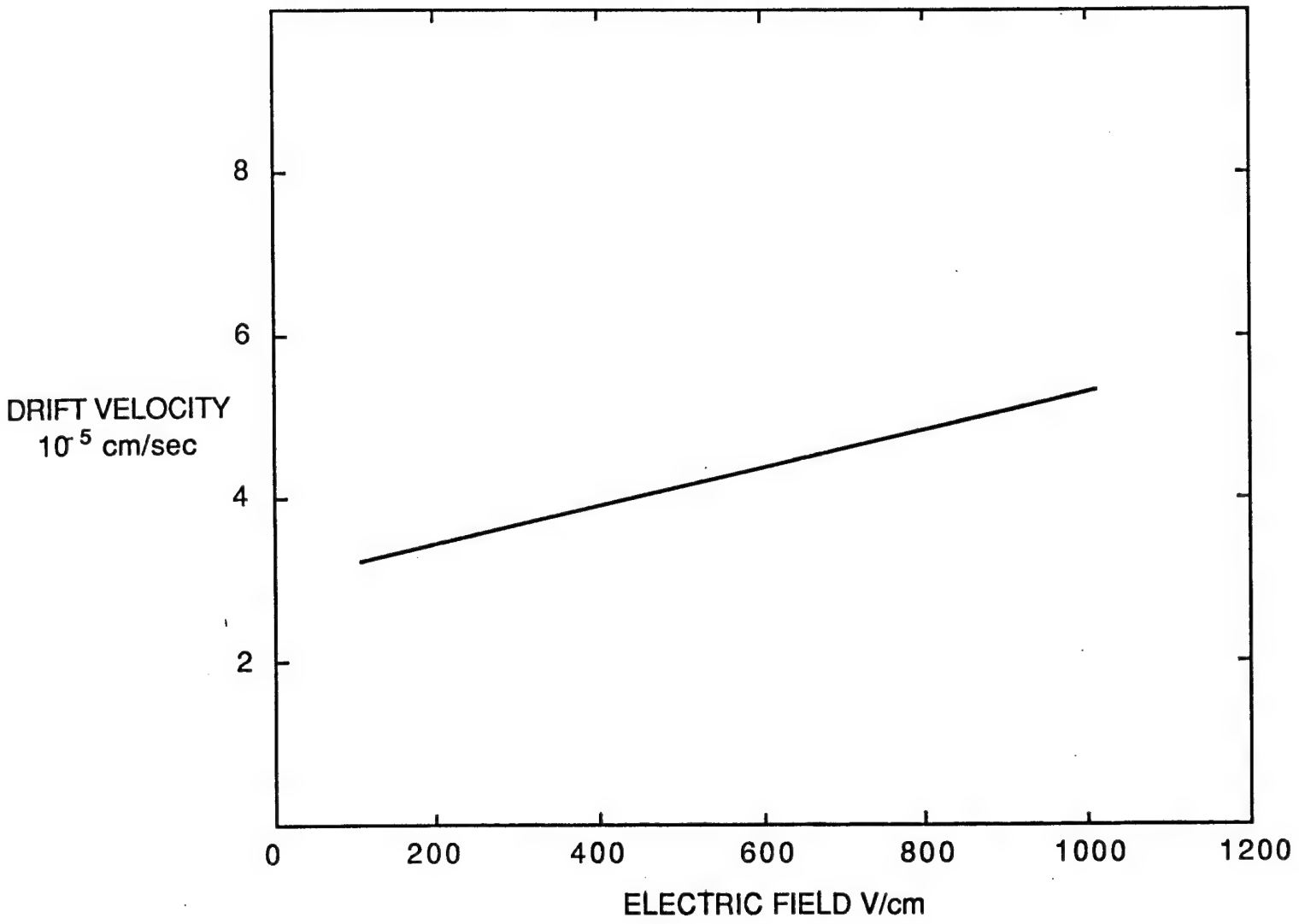

Figure 6: Electron drift velocity as a function of the discharge electric field.

to 30 meters should not be an issue. The appropriate architecture for scaling to very high power is the expanding wave architecture. Such a laser architecture, already demonstrated by SRL for excimer lasers under an SDIO/ONR program, can be used to maintain high efficiency as the laser length is increased to provide higher average power. The expanding wave laser architecture will also reduce the effects of amplified spontaneous emission on the performance of large scale rare gas laser amplifiers. Therefore, length scaling of rare gas laser power amplifiers is likely to be constrained by medium homogeneity and its impact on laser beam quality and ultimately by optical damage. At a laser length of 30 m, a medium homogeneity, $\Delta\rho/\rho$, of 2×10^{-5} is required to preserve laser beam quality. This homogeneity has already been demonstrated in small scale flow loops developed for excimer lasers. Ultimately laser length scaling will be constrained by the fluence and average intensity which can be processed by the output window of the amplifier. For a conventional amplifier architecture, the average output intensity is 4 KW/cm^2 and the single pulse fluence is 150 J/cm^2 for a 100 MW laser design. At near IR wavelengths, these levels are within current state-of-the- art. These levels can be reduced by a factor of 2 by using an expanding wave laser amplifier architecture.

5.0 STABILITY OF ELECTRON BEAM PUMPED RARE GAS DISCHARGES

Discharge methods for pumping rare gas lasers fall into three categories: self sustained discharges, UV/X-ray preionized discharges and electron beam controlled discharges. Of these, the electron beam controlled discharge is the most stable and is the only discharge method that can be scaled to the high average powers required for strategic applications.

The reason that electron beam controlled discharges are more stable than other discharge methods is that essentially all of the secondary electron production is due to the high energy electron beam. The discharge electric field can then be adjusted to optimize the laser efficiency. In self-sustained and preionized laser discharges, the applied electric field has to be sufficiently large to allow production of secondary electrons by direct ion-

ization of the laser mixture by discharge electrons and also to allow efficient excitation of the upper laser level. Typically the electric field required for ionization is substantially larger than that required for the excitation of the upper laser level; in fact it is usually sufficiently large to result in instability and arcing and therefore the electron beam controlled discharge, which decouples ionization and excitation, is the preferred approach.

Rare gas discharges have been investigated in detail for several years and it has been shown[4] conclusively that the stability of these discharges are dominated by multi step ionization processes in which the first electron produces a rare gas metastable and a second electron ionizes the metastables. Cross-sections for ionization of the rare gas metastables by electron impact are large, of order $10\mathring{A}^2$, since these metastable states are electronically similar to the adjacent alkalis in the periodic table. From the previous discussions on the physics of discharge pumping, the required metastable density was 5×10^{13} cm^{-3}. So for a total pressure of 3 atm, the ratio of the metastable density to the ground state density is 10^{-6}. Boltzmann code calculations predict that the electron impact ionization rate of the metastables is two orders of magnitude larger than the ground state ionization rate at these fractional metastable densities.

The discharge model that has been analysed during Phase I is shown schematically in Fig. 7. There are two excited states n_m and n_2 and the ionization of Xe. n_m is the xenon metastable states, n_2 represents the 6 p levels of Xe, and quasis neutrality of the discharge demands that n_i and the electron density n_e are equal. The time rate of charge of these three species are given by

$$\frac{dn_m}{dt} = S_m - \frac{n_m}{\tau_m} - \gamma 12 n_e n_m + \gamma 21 n_e n_2 + R n_2 + \langle \sigma \nu \rangle n_e n_a \tag{10}$$

$$\frac{dn_2}{dt} = S_2 + \gamma 12 n_e n_m - \gamma 21 n_e n_2 - R n_2 - \nu n_2 + \alpha n_e^2 \tag{11}$$

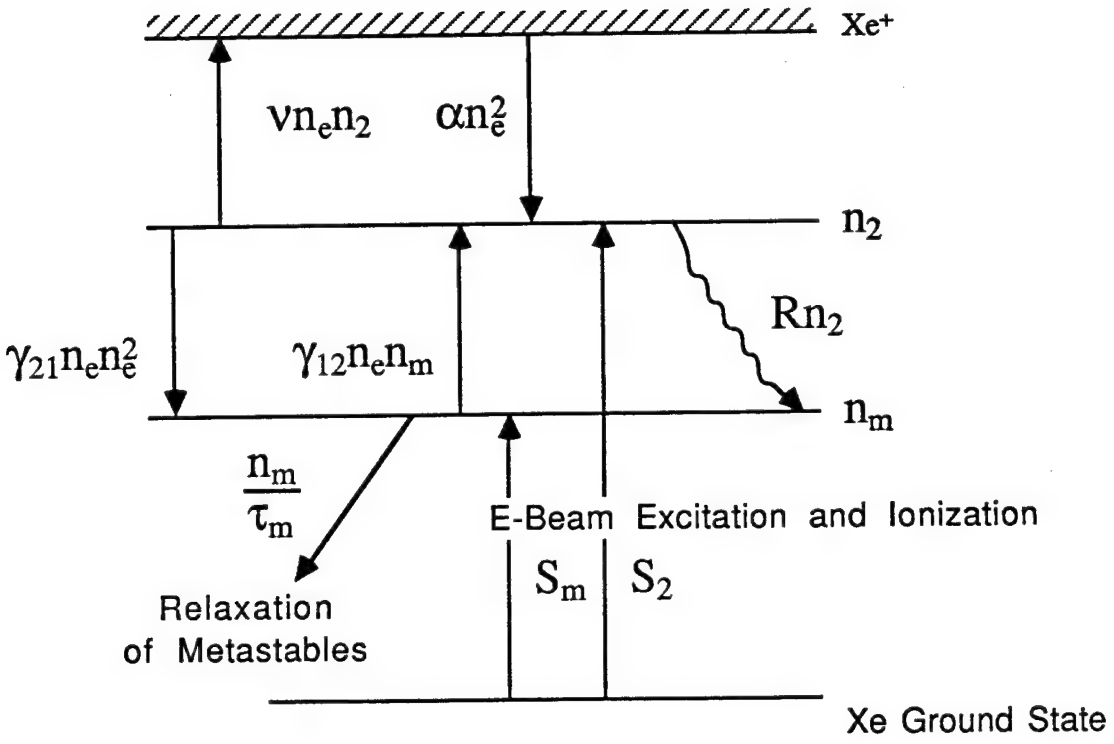

Figure 7: Schematic showing the various excited states and reactions used in the discharge model.

$$\frac{dn_e}{dt} = S_{eb} + \nu n_e n_2 - \alpha n_e^2 \tag{12}$$

Where n_e is the electron density, S_{eb} is the electron beam ionization rate, n_m is the metastable density, α is the recombination rate, $\langle \sigma v \rangle$ is the electron impact metastable production rate constant and τ_m is the metastable lifetime,S_m and S_2 are the direct excitation of metastables by the electron beams. γ_{12} is the electron excitation rates from the metastable level Xe* to Xe** and γ_{21} is the reverse process. R is the total decay rate (including collisional quenching and radiative decay) of n_2 to $n_m \cdot$ ν is the ionization rate of n_2. In writing Eqs. (10), (11) and (12) it has been assumed that this ionization rate is dominant because it requires only 3 eV to ionize n_2 while it requires 4.5 eV to ionize Xe*(n_m) and 13.5 eV to ionize the ground state of Xe. Hence most of the electrons can ionize n_2. This fact combined with the fact that n_2 has the largest ionization cross-section of the three states results in the ionization of n_2 being the dominant ionization.

Equations (10) and (11) can be added to give

$$\frac{d}{dt}(n_m + n_2 + n_e) = S_m + S_2 + S_{eb} - \frac{n_m}{\tau_m} + \langle \sigma \nu \rangle n_e n_a \tag{13}$$

$S_{eb} >> S_m, S_2$ and $\langle \sigma \nu \rangle n_e n_a$, hence the steady state density of n_m, n_{mo} is given by

$$n_{mo} \simeq \tau_m (S_{eb} + \langle \sigma \nu \rangle n_{eo} n_a) \tag{13a}$$

By substituting this value of n_{mo} into Eq. (11) one finds that the steady state density of n_2 is

$$n_{20} = \frac{S_{eb}(\tau \gamma_{12} n_{eo} + 1) + \tau \gamma_{12} n_{eo}^2 n_a \langle \sigma \nu \rangle}{\gamma_{21} n_{eo} + R} \tag{14}$$

By substituting Eqs. (13) and (14) into (12) one gets

$$S_{eb}\left[1 + \frac{\nu n_{eo}(\tau_m \gamma_{12} n_{eo} + 1)}{(\gamma_{21} n_{eo} + R)}\right] + n_{eo}^2 \left\{ \frac{\nu \tau_m \langle \sigma \nu \rangle n_a \gamma_{12} n_{eo}}{\gamma_{21} n_{eo} + R} - \alpha \right\} = 0 \tag{15}$$

Typically the electron mixing rate $\gamma_{12} n_{eo}$ is very rapid and as a result Eq. (15) simplifies to

$$S_{eb}\left[1+\nu\tau_m n_{eo}\right]+(\nu\tau_m\langle\sigma\nu\rangle n_a-\alpha)n_{eo}^2-\alpha n_{eo}^2=0 \tag{16}$$

So the steady state electron density is given by

$$n_{eo}=\left[\nu S_{eb}\tau_m+\left\{(S_{eb}\nu\tau_m)^2+4S_{eb}(\alpha-\langle\sigma\nu\rangle n_a\tau_m)\right\}^{1/2}\right]\Big/2(\alpha-\langle\sigma\nu\rangle n_a\tau m) \tag{17}$$

From Eq. (17) it is apparent that for a steady state solution to the discharge Eqs. (10), (11), and (12)

$$\alpha>\langle\sigma\nu\rangle n_a\tau_m \tag{18}$$

As the electric field increases α decreases and $\langle\sigma\nu\rangle$ increases and so condition (18) is satisfied below some critical electric field E_c. For the conditions given in Table 2 of this proposal and using the rate constants predicted by the Boltzmann code $E_c = 900$ V/cm so one must operate the discharge below 900 V/cm. Using the rates predicted by the Boltzmann code (see Figs. 3-5) in Eqs. (13) and (14) one can estimate the steady state values n_{mo}, n_{20} and n_{eo} as a function of S_{eb}. These results are plotted in Figs. 8 and 9. From these figures one can see that for an S_{eb} of 10^{20} cm^{-3} sec^{-1} the steady state metastable n_{mo} and secondary electron densities n_{eo} are consistent with Table 2.

Having obtained the steady state densities of the metastables and electrons, the stability of these values will be discussed neet by performing a perturbation expansion about the steady state values. i.e

$$n_m(t)=n_{mo}+\delta_m(t)$$

$$n_2(t)=N_{20}+\delta_2(t)$$

$$n_e(t)=N_{eo}+\delta_e(t)$$

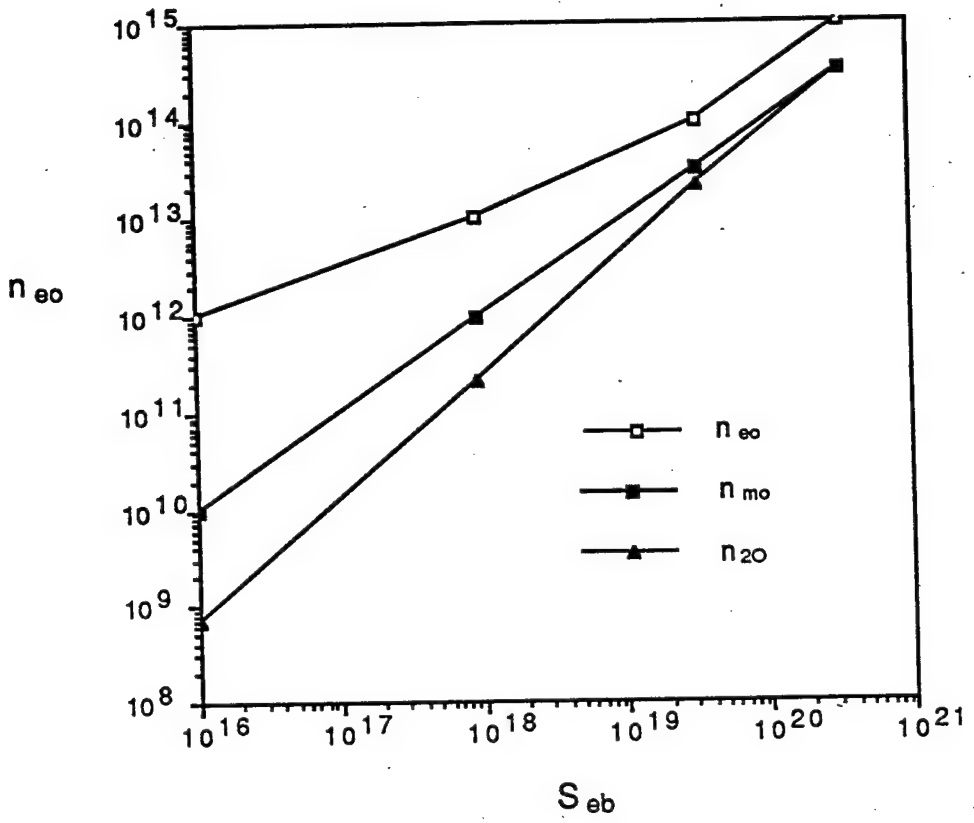

Figure 8: Curves showing the variation of n_{eo}, n_{mo}, n_{20} as a function of S_{eb} for an applied electric field of 300 V/cm.

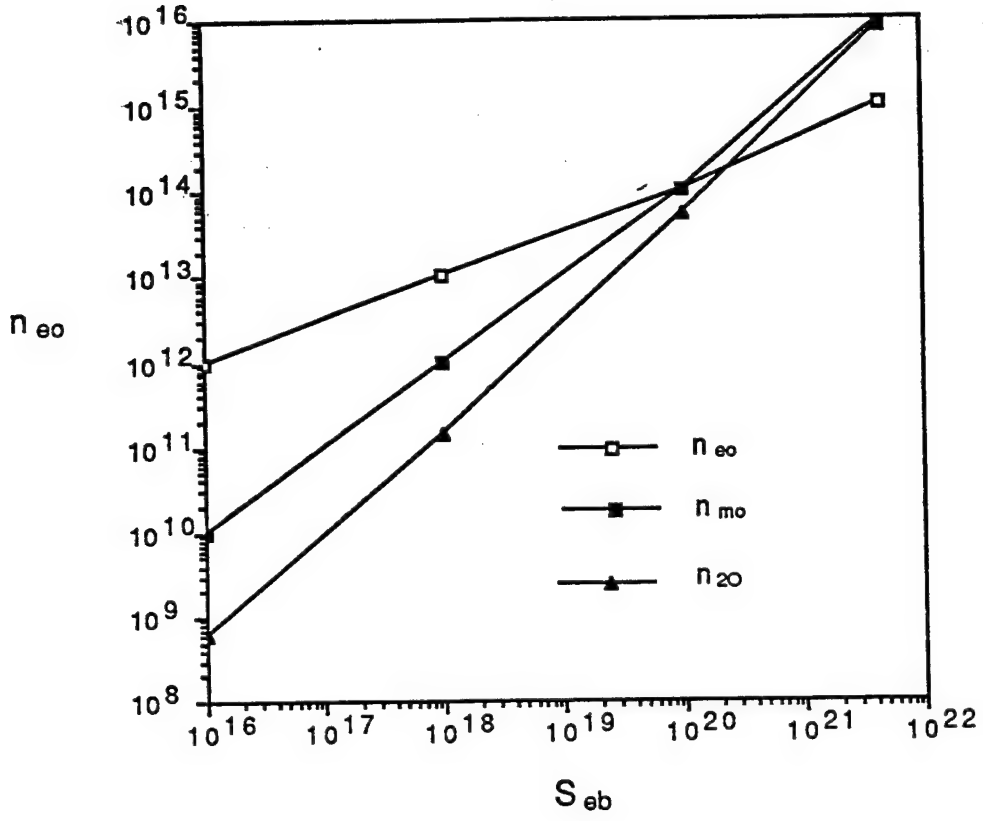

Figure 9: Curves showing the variation of n_{eo}, n_{mo}, n_{20} as a function of S_{eb} for an applied electric field of 700 V/cm.

This expansion is substituted into Eqs. (10) and (12). Assuming that voltage across the discharge does not vary one obtains the following first order linearized equations

$$i\omega\delta_m = -\gamma_{12}(n_{mo}\delta_e + n_{eo}\delta_m) - \frac{\delta_m}{\tau_m} + \gamma_{21}(\delta_2 n_{eo} + \delta_e n_{20}) + RS_2 + \langle\sigma\nu\rangle n_a\delta_e \tag{19}$$

$$-i\omega\delta_2 = \gamma_{12}(n_{mo}\delta_e + n_{eo}\gamma_m) - \gamma_{21}(\delta_2 n_{eo} + \delta_e n_{20}) - R\delta_2 + 2\alpha n_{eo}\delta_e \tag{20}$$

$$-i\omega\delta_e = \nu\delta_2 n_{eo} + \nu n_{20}\delta_e - 2\alpha n_{eo}\delta_e \tag{21}$$

The $(-i\omega)$ on the RHS of Eqs. (19),(20) and (21) are the result of a Laplace transform of the linearized equations.

The characteristic matrix for this system is given by

$$\vec{D}_{cu} = \begin{bmatrix} x + a_{11} & a_{12} & a_{13} \\ a_{21} & x + a_{22} & a_{23} \\ 0 & a_{32} & x + a_{33} \end{bmatrix} \tag{22}$$

where

$$a_{11} = \gamma_{12}n_{eo} + 1/\tau$$

$$a_{12} = -(\gamma_{21}n_{eo} + R)$$

$$a_{13} = \gamma_{12}n_{10} - \gamma_{21}n_{20} + \langle\sigma\nu\rangle n_a$$

$$a_{21} = -\gamma_{12}n_{eo}$$

$$a_{22} = \gamma_{21}n_{eo} + R + \nu n_{eo} \tag{23}$$

$$a_{23} = -\gamma_{12}n_{10} + \gamma_{21}n_{20} - 2 \propto n_{eo} + \nu n_{20}$$

$$a_{32} = -\nu n_{eo}$$

$$a_{33} = 2\alpha n_{eo} - \nu n_{20}$$

The characteristic equation in this case is

$$(x+a_{33})[(x+a_{11})(x+a_{22})-a_{12}a_{21}]-a_{32}[(x+a_{11})a_{23}-a_{21}a_{13}] = x^3+Ax^2+Bx+C = 0 \tag{24}$$

where

$$A = a_{11} + a_{22} + a_{33}$$

$$B = a_{11}a_{22} + a_{11}a_{33} + a_{22}a_{33} - a_{12}a_{21} - a_{23}a_{32}$$

$$C = a_{11}a_{22}a_{33} + a_{32}a_{21}a_{13} - a_{32}a_{11}a_{23} - a_{12}a_{33}a_{21}$$

The conditions for **all** the roots of Eq. (24) to have a **negative** real part (stable conditions) are

$$B; C; D = AB - C > 0 \tag{25}$$

The coefficients A, B, C and D have been computed for the three cases considered previously and the results are shown below:

	n_e	10^{12}	10^{13}	10^{14}	10^{15}
	A	$2{\cdot}10^{7}$	$2.5{\cdot}10^{7}$	$6.7{\cdot}10^{7}$	$4.8{\cdot}10^{8}$
E=300 V/cm	B	$2{\cdot}10^{13}$	$2.7{\cdot}10^{13}$	$1.7{\cdot}10^{13}$	$9{\cdot}10^{15}$
	C	$4{\cdot}10^{17}$	$4.4{\cdot}10^{18}$	$8.3{\cdot}10^{20}$	$4.5{\cdot}10^{21}$
	D	$4.4{\cdot}10^{20}$	$6.9{\cdot}10^{20}$	$1.1{\cdot}10^{22}$	$4.3{\cdot}10^{24}$
	A	$2.1{\cdot}10^{7}$	$3{\cdot}10^{7}$	$1.1\cdot10^{8}$	$9.4{\cdot}10^{8}$
E=700 V/cm	B	$2.1{\cdot}10^{13}$	$3.2{\cdot}10^{13}$	$3.3{\cdot}10^{14}$	$2.3{\cdot}10^{16}$
	C	$4.1{\cdot}10^{17}$	$4.6{\cdot}10^{18}$	$7.2{\cdot}10^{19}$	$4.6{\cdot}10^{22}$
	D	$4.6{\cdot}10^{20}$	$9.5{\cdot}10^{20}$	$3.7{\cdot}10^{22}$	$2.1{\cdot}10^{25}$

The conclusion is that the discharge is absolutely stable under the conditions considered.

To verify these conclusions the Eqs. (10), (11) and (12) have been numberically intergrated and the results are shown in Figs. 10, 11 and 12 for electric fields of 300 V/cm, 700 V/cm and 1500 V/cm. In all three cases S_{eb} was assumed to be 10^{20} cm^{-3} sec^{-1}. As one can see from Figs. 10 and 11 a stable steady state is reached for the lower electric

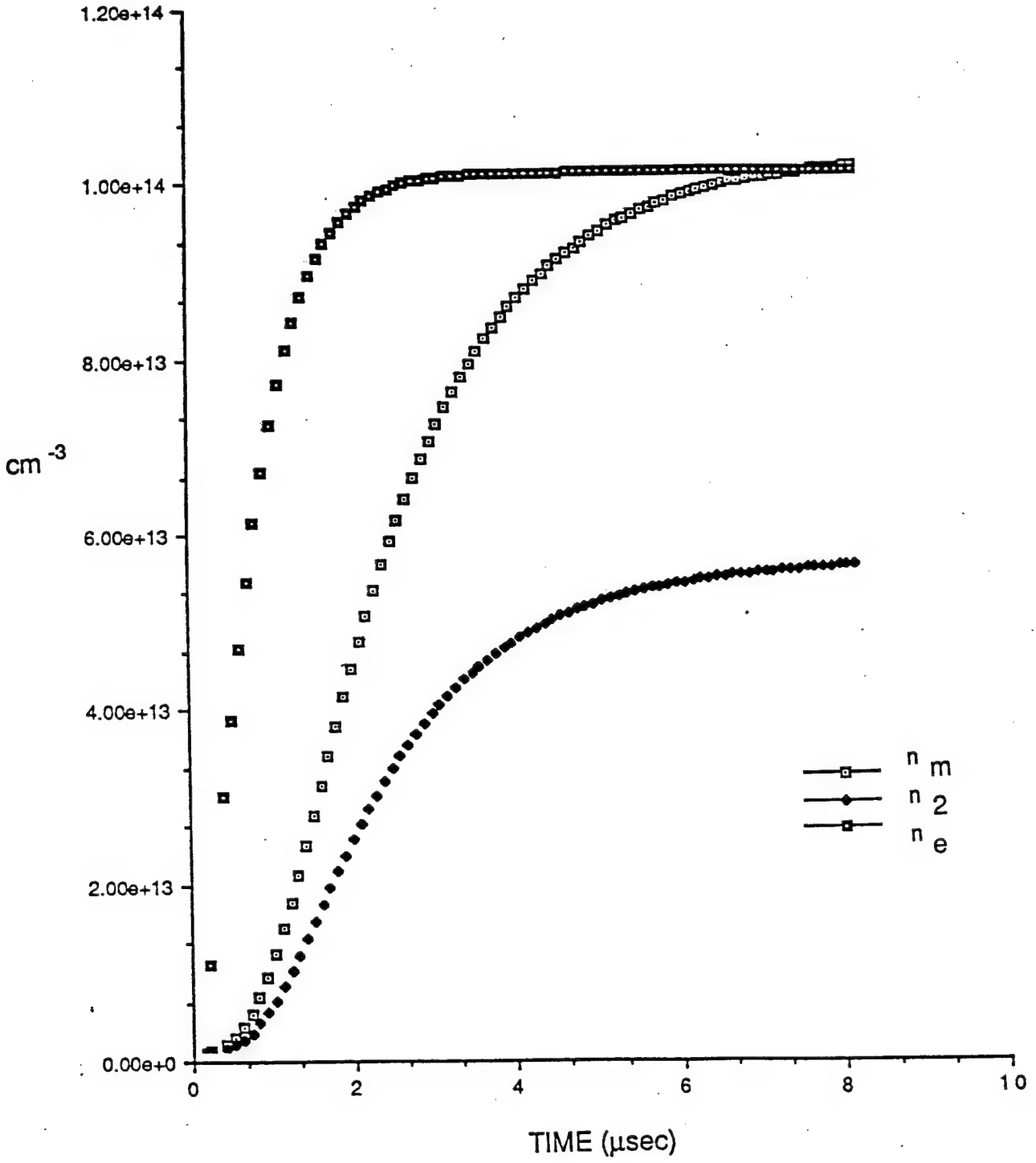

Figure 10: Curves showing the temporal variation of n_{eo}, n_{mo}, n_{20} for an applied electric field of 300 V/cm.

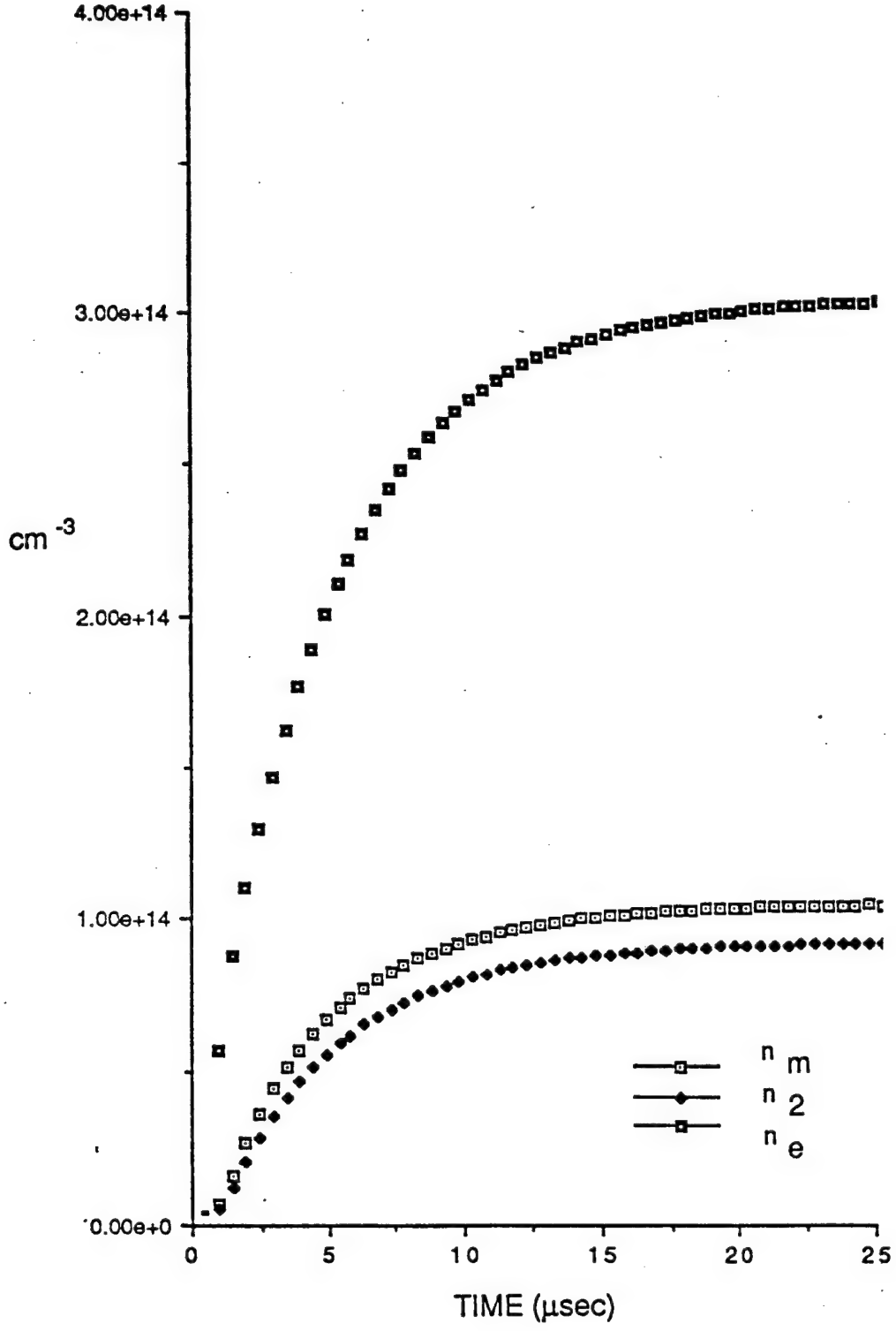

Figure 11: Curves showing the temporal variation of n_{eo}, n_{mo}, n_{20} for an applied electric field of 700 V/cm.

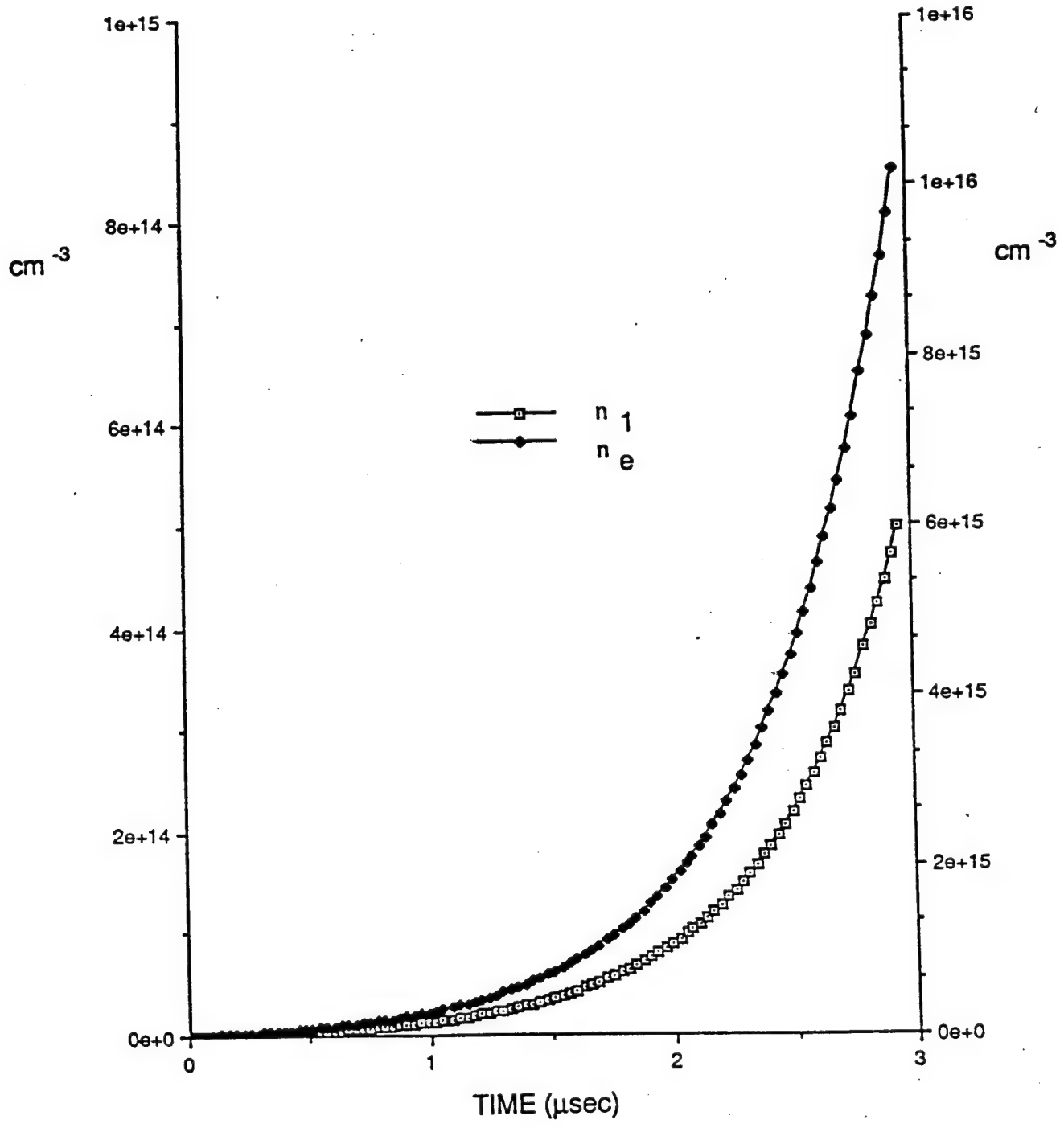

Figure 12: Curves showing the temporal variation of n_{eo}, n_{mo}, n_{20} for an applied electric field of 1500 V/cm.

fields 300 and 700 V/cm. The steady state values of n_{eo}, n_{mo} and n_{20} are consistent with the predictions shown in Figs. 8 and 9. When the electric field is raised to 1500 V/cm a steady state is not reached this is because the condition given by Eq. (18) is violated and no steady state solution exists.

6.0 Modeling of the 1.73μm Ar/Xe Laser

In order to gain insight into the important parameters governing operation of the 1.73μm Ar/Xe laser system a simplified rate equation model is being developed. This model is outlined in Fig. 13. The upper laser level (Level 2) is pumped via recombination of electron-ion pairs. Collisions between electrons and Xe atoms cause transitions at the rate τ_{e3}^{-1} back to the continuum, at rate τ_{e2}^{-1} from the upper laser level down to the lower laser level (superelastic collisions), and collisional excitation at the rate τ_{e1}^{-1}. Lumped loss rates from both levels to lower lying energy levels are included as rates τ_2^{-1} and τ_1^{-1}. For convenience, the collisional rates out of the upper laser level are expressed as ratios to the collisional excitation rate into the upper level from the lower level.

$$\text{Asym} \equiv \frac{\tau_{e1}}{\tau_{e2}} \tag{26}$$

$$\text{Fn} \equiv \frac{\tau_{e1}}{\tau_{e3}} \tag{27}$$

The rate equation set then becomes

$$\frac{dN_2}{dt} = \alpha n_e^2 - \frac{g\phi}{h\nu} + \tau_{e1}^{-1}\left[N_1 - N_2(\text{Asym} + \text{Fn})\right] - \tau_2^{-1}N_2 \tag{28}$$

$$\frac{dN_1}{dt} = \frac{g\phi}{h\nu} + \tau_{e1}^{-1}\text{Asym} \cdot N_2 - N_1(\tau_{e1}^{-1} + \tau_1^{-1}) \tag{29}$$

$$\frac{dn_e}{dt} = \frac{P(t)}{E_{eff}} - \alpha n_e^2 + \tau_{e1}^{-1}\text{Fn} \cdot N_2 \tag{30}$$

where the small signal gain g is defined by

$$g \equiv \sigma_s\left[N_2 - N_1(g_l/g_u)\right] \tag{31}$$

where N_2 and N_1 are the upper and lower laser level population densities, respectively, n_e is the electron density, $h\nu$ is the photon energy (0.72 eV), σ_s is the stimulated emission

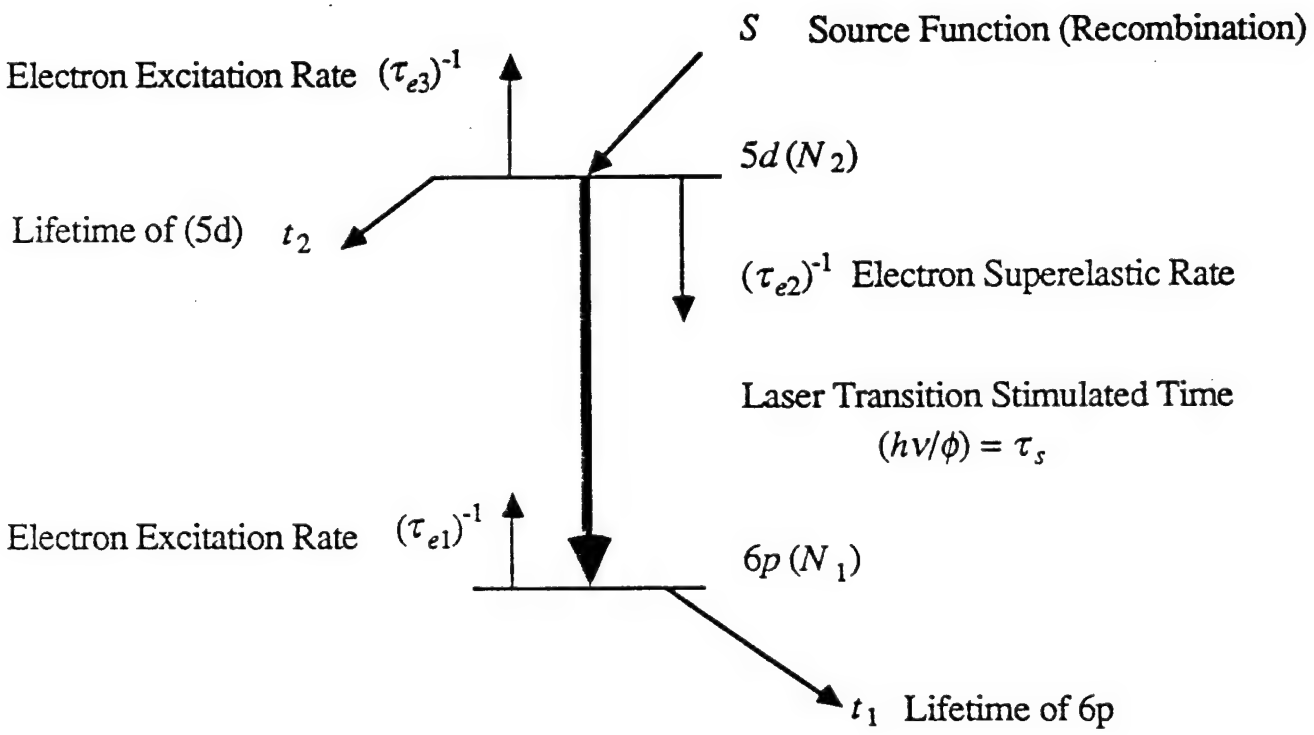

Figure 13: Simplified ArXe laser model

cross section and g_u and g_l are the upper and lower level degeneracies. Completing this system is the cavity optical flux equation given by

$$\frac{d\phi}{dt} = c\phi\left[\mathrm{F_{cav}}g + \frac{1}{2\mathrm{L}}(\ln R - C_{loss})\right] + \phi_{\mathrm{spon}} \tag{32}$$

where the factor $\mathrm{F_{cav}}$ is required since in the experiments performed to date the the electron beam was masked to pump less than the full length of the optical cavity. The effects of amplified spontaneous emission were minimized by this technique. The form of the cavity flux equation used as Eq. (32) is valid if the cavity round trip time (2L/c) is short compared to other significant times scales of the system.

These equations may be integrated numerically using standard techniques (e.g., a Gear method). The recombination coefficient (α) may have a time dependance since it is a strong function of the electron temperature. This may be especially important in the afterglow period of the discharge. The results discussed here were obtained using a constant value of α. Numeric difficulties may be avoided by normalizing the equation set by appropriate scale factors. Boldface dimensionless quantities are defined by the following expressions

$$N_i = \mathrm{N_i}(\alpha/k)\, n_{char}, \quad i = 1,2 \tag{33}$$

$$n_e = \mathrm{n_e} n_{char} \tag{34}$$

$$\phi = \mathbf{\Phi}\,(k \cdot n_{char} h\nu/\sigma_s) \tag{35}$$

$$t = \mathbf{T}/\,(k \cdot n_{char}) \tag{36}$$

where

$$\tau_{e1}^{-1} = k \cdot n_e \tag{37}$$

and

$$n_{char} = (P_0/\alpha E_{eff})^{1/2} \tag{38}$$

$$P(t) = P_0 \cdot f(t)$$

where $P(t)$ is the electron beam pumping power per unit volume (P_0 is the peak pump rate) and E_{eff} is the averaged energy expended per electron ion pair. The factor n_{char} is the electron density reached in steady state in the absence of supraelastic collisions from the upper laser level (Fn=0). The normalized equation set then becomes

$$\frac{d\mathbf{N_2}}{d\mathbf{T}} = \mathbf{n_e}^2 - \mathbf{\Phi}\left[\mathbf{N_2} - \mathbf{N_1}(g_l/g_u)\right] + \mathbf{n_e}\left[\mathbf{N_1} - \mathbf{N_2}(\mathrm{Asym} + \mathrm{Fn})\right] - \frac{\mathbf{N_2}}{(kn_{char}\tau_2)} \tag{39}$$

$$\frac{d\mathbf{N_1}}{d\mathbf{T}} = \mathbf{\Phi}\left[\mathbf{N_2} - \mathbf{N_1}(g_l/g_u)\right] + \mathrm{Asym}\cdot\mathbf{n_e N_2} - \mathbf{n_e N_1} - \frac{\mathbf{N_1}}{(kn_{char}\tau_1)} \tag{40}$$

$$\frac{d\mathbf{n_e}}{d\mathbf{T}} = (\alpha/k)(f(t) - \mathbf{n_e}^2 + \mathrm{Fn}\cdot\mathbf{n_e N_2}) \tag{41}$$

$$\frac{d\mathbf{\Phi}}{d\mathbf{T}} = \mathbf{\Phi}\left\{F_{cav}\left[\mathbf{N_2} - \mathbf{N_1}(g_l/g_u)\right] + \frac{c}{(2Lkn_{char})}(\ln R - C_{loss})\right\} + \frac{\phi_{spon}\sigma_s}{(k^2 n_{char}^2 h\nu)} \tag{42}$$

Finally, an expression for the spontaneous emission rate into the laser optical mode is required. The form derived by Siegman (written in terms of the cavity flux rather than the photon number) is

$$\phi_{spon} = \frac{N_2 h\nu c^2 \sigma_s}{2V} \tag{43}$$

where V is the volume occupied by the mode. Substituting for the fundamental mode cross sectional area of a half-symmetric (plano-concave) optical cavity allows the spontaneous emission to be written as a function of the mirror radius of curvature (R_{mir}).

$$\phi_{spon} = \frac{N_2 h\nu c^2 \sigma_s}{2L(LR_{mir})^{1/2}\lambda(1 - L/R_{mir})^{1/2}} \tag{44}$$

These equations can then be solved with an appropriate choice for the pump rate function $f(t)$.

The dimensionless output flux is given by

$$\mathbf{\Phi_{out}} = \mathbf{\Phi}(1 - R)/2 \tag{45}$$

where R is the output coupler reflectivity. The feedback coupler is assumed to be a high reflector with the total optical cavity losses included as C_{loss}.

The steady state solution of Eq. (39-41) can provide information on the small signal gain and the saturation flux as a function of the mosel parameters. The small signal gain is found by setting $\Phi = 0$ and solving the equation set algebraically.

The saturation flux is defined as the steady state flux which reduces the the gain to half of the small signal ($\Phi \rightarrow 0$) level. The parameters Asym and Fn must be determined via an iterative process using experimentally determined values for the small signal gain g and the saturation flux ϕ_{sat} at several pump powers as a check. A Rigrod analysis of the time integrated pulse energies for three different electron beam pump powers has been performed. Values of the parameters $\tau_1, \tau_2, k,$ and α were estimated and fixed to the following values.

$$\tau_1 = 40\,\text{nsec} \tag{46}$$

$$\tau_2 = 270\,\text{nsec} \tag{47}$$

$$\alpha = 2 \times 10^{-13}\text{m}^3\text{sec}^{-1} \tag{48}$$

$$k = 2 \times 10^{-13}\text{m}^3\text{sec}^{-1} \tag{49}$$

Regions in the Asym-Fn plane which correspond to values of g and ϕ_{sat} within some selected range of the experimentally measured values may be found by imposing one further constraint. It was found that using a theoretical estimate of the stimmulated emission cross section ($\sim 10^{-13}\,\text{cm}^2$) resulted in gains a factor of 10^2 too large. Therefore, the small signal gain at the lowest pump power investigated (2.2 kW/cm^3) was fixed at 0.038 cm^{-1} by adjusting the cross section for each choice of Asym and Fn. The results of such a process are shown as Fig. 14 where regions which predict values within 10% of the experiment are delineated for each of the pump powers employed (2.2, 6.8, and 16.2 kW/cm^3). It has been found that choosing Asym= 1.77 (which would correspond to $T_e = 1.2$ eV using detailed balancing arguments) and Fn= 0.8 and solving the time dependant equations Eq.

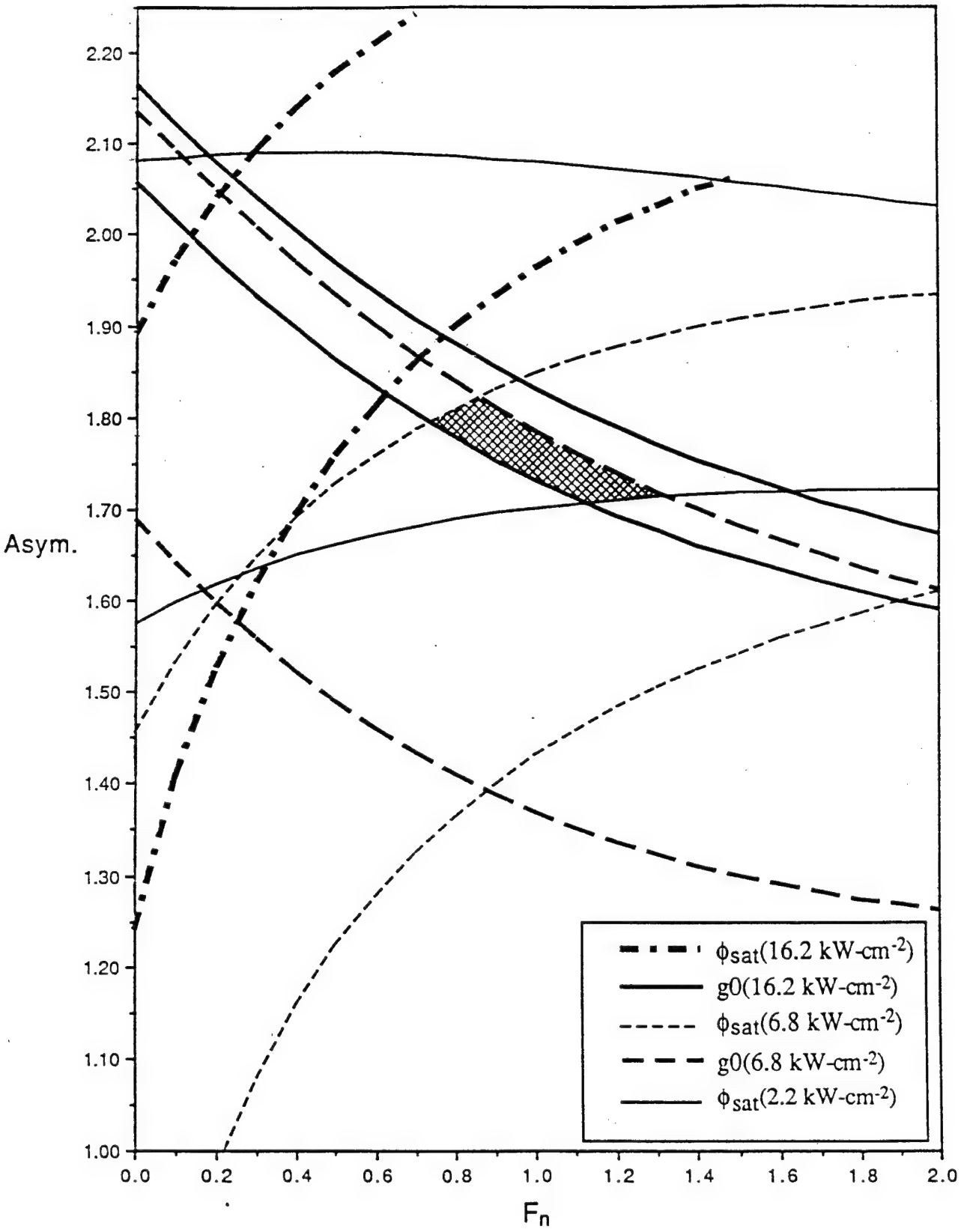

Figure 14: Regions in the Asym. - F_n plane for which a steady state value of a derived variable lies within 10% of the experiment. Contours bounding the regions for small signal gain and saturation flux for three pump powers are shown.

(39-41) that the calculated pulse energies match the experiment well. Figure 15 shows a comparison of calculated and measured pulse energies at a pump power of 2.2 kW. While the integrated energies are predicted the detailed transient pulse behavior does not yet match well. Further work on the model to improve its capability is under way. An acceptable model will permit rapid predictions of scaling behavior.

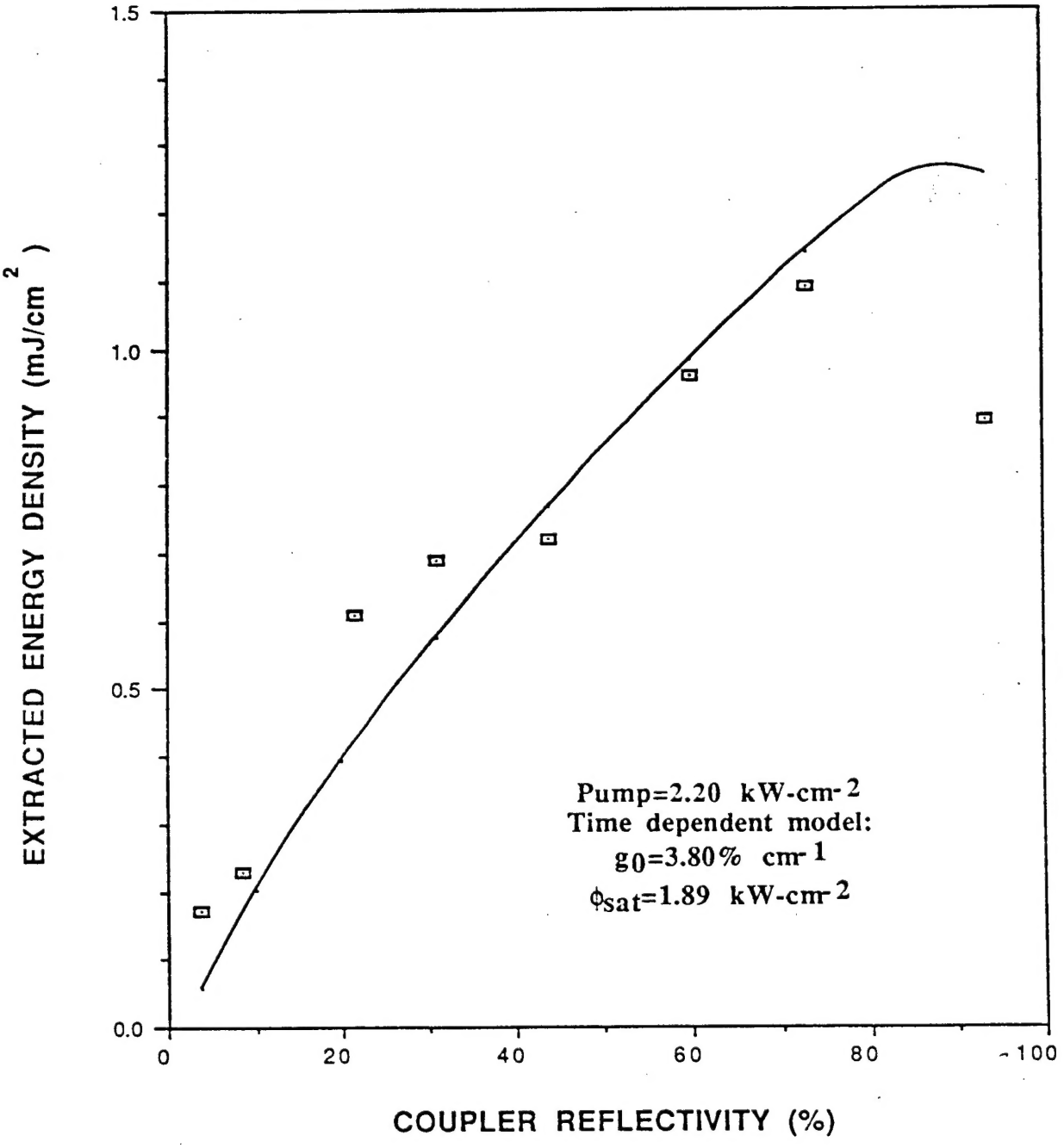

Figure 15: Comparison of calculated and measured ArXe extraction, 50 cm gain length, 10 m/flat cavity, and 0.5% Xe in Ar.

CONCLUSION

SRL has analysed both the stability of the rare gas discharge and the kinetics of the Ar/Xe laser. The electron beam controlled discharge is absolutely stable provided that the electric field is below a critical value. From the analysis of existing laser data, it is clear that the electron kinetics have a significant effect on the Ar/Xe laser . Because of the rapid electron mixing rates, the rare gas lasers tend to operate less efficiently at higher pump powers.

REFERENCES

1. N.G. Basov et al, IEEE Journal of Quantum Electronics QE21, 1756 (1985).

2. Sandia Group - private communication (1988).

3. NRL Group - private communication (1988).

4. J.A. Mangano and J.H. Jacob, Appl. Phys. Lett. 28, 581 (1976).